공학석사 학위논문

Fabrication of 3D Chiral Plasmonic Patterns and their Applications

3차원 카이랄 플라즈모닉스 패턴의 제조 및 응용

2021년 02월

서울대학교 대학원

화학생물공학부 고분자 및 유기 소재 전공

원 유 상

Fabrication of 3D Chiral Plasmonic Patterns and their Applications

3차원 카이랄 플라즈모닉스 패턴의 제조 및 응용

지도교수 오 준 학

이 논문을 공학석사 학위논문으로 제출함

2021년 02월

서울대학교 대학원

화학생물공학부 고분자 및 유기 소재 전공

원 유 상

원유상의 공학석사 학위논문을 인준함

2021년 02월

위 원 장 이 종 찬 (인)

부위원장 오 준 학 (인)

위 원 유 동 원 (인)

Abstract

Fabrication of 3D Chiral Plasmonic Patterns and their Applications

Won You Sang
School of Chemical and Biological Engineering
The Graduate School
Seoul National University

Artificial chiral structures including from 2D to metasurface and 3D have received significant attention because of their unique optical characteristics. However, the realization of nano-scale and even micro-scale chiral structures has still been an issue due to the complicated fabrication process and limitation of material.

In this work, we fabricate 3D chiral plasmonic patterns (CPPs) by symmetric biaxial stretching with nano-scale grating-patterned PDMS film. The novel 3D CPPs have micro-scale chiral patterns, nano-scale grating patterns, and the other nano-scale irregular patterns. And the 3D CPPs are analyzed for potential applications for reflective display. Incorporating 3D CPPs as a back reflector in reflective display has shown the possibility that changes in optical properties due to the different interactions between the structures and either left-handed or right-handed circularly polarized light can be seen as a color change. This method could be widely utilized for the fabrication of multi-patterned 3D chiral structures.

Keywords : Chirality detection, Plasmonic Effect, Chiral Plasmonic Patterns, Reflective Display

Student Number : 2019-29299

Table of Contents

List of Figures and Tables

Chapter 1. Introduction

1.1 Chirality

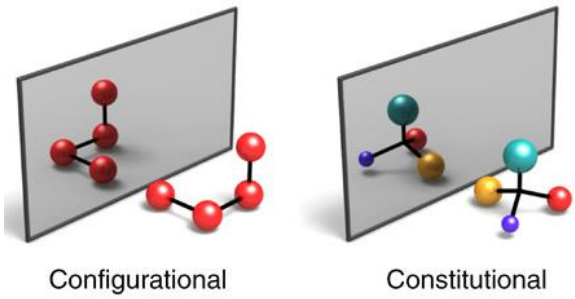

Figure 1. Chirality from configuration or constitution. (ref. 1)

Objects are called *chiral*, the Greek word for "handed," if they are non-superimposable mirror images of each other (**Figure 1**). Describing from a mathematical point of view, chiral objects cannot have mirror planes. And this geometric property is called *chirality*.[1] Chirality exists naturally in many different kinds of biomolecules: the essential amino acids, carbohydrates, nucleic acids, proteins are examples from nature. Many drug molecules are also chiral molecules. Between them, only one enantiomer, is suitable for the disease therapy while the other one being functionless or even toxic.[2] Therefore, it is extremely important to develop convenient and efficient techniques for chirality detection. However, mirror-image molecules have almost the same physical properties. So, physical methods can hardly be applied to the separation between mirror-image molecules.[3]

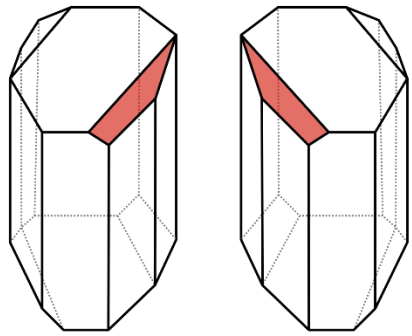

Figure 2. Left and right crystal shapes separated by Pasteur. In solution, one form rotated light to the left, the other to the right while an equal mixture (racemic mixture) of the two forms canceled each other's effect, and does not rotate the linearly polarized light. (ref. 4)

Since Pasteur discovered the molecular chirality in 1848, it has been understood that the two enantiomers of chiral molecules interact differently with polarized light (**Figure 2**).[4] As a result, optical techniques are widely used to detect chirality. For example, *polarimetry* is a common method used to distinguish between enantiomers, based on their ability to rotate a linearly polarized light (or plane-polarized light) in opposite directions. This is due to *circular birefringence* (CB) effect and can be explained by the difference in the real part of the refractive index. In addition, chiral molecules have a different absorption of the left circularly polarized light (*L*-CPL) or right circularly polarized light (*R*-CPL), which is called *circular dichroism* (CD). This is can be explained by the difference in the imaginary part of the refractive index. (CB, CD, L-CPL and R-CPL will be discussed in more detail in **Chapter 1.4**, **1.5**.)

1.2 Plasmonics

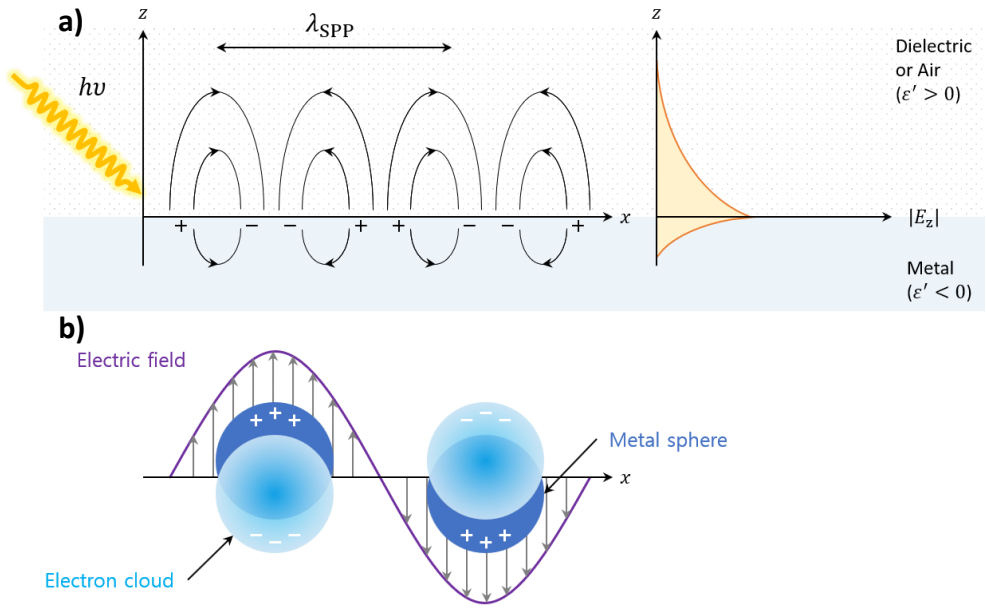

Figure 3. Schematic diagrams for a) surface plasmon-polaritons (SPPs) and b) localized surface plasmons (LSPs)

Plasmon refers to a quasi-particle in which free electrons in a metal vibrate as a group. Surface plasmon resonance (SPR) is a combination of electromagnetic waves and plasmon, and generates locally enhanced electric field. This means that surface plasmon-polaritons (SPPs) are produced by combining plasmon and photon. The generated SPPs have the property of electromagnetic waves that propagate along the interface between a negative-permittivity material (metal, $\varepsilon' < 0$) and a positive-permittivity one (dielectric material or air, $\varepsilon' > 0$) (**Figure 3a**). The SPR effect exhibits light energy is converted into surface plasmons and accumulated on the surface of metal nanoparticles so that light can be controlled in a region smaller than the

diffraction limit of light.

There are two types of SPR phenomena: propagating surface plasmon resonance (PSPR) observed at the interface between planar metal layer (thickness: 10~200 nm) and dielectric layer, and localized surface plasmon resonance (LSPR) observed in 10 to 200 nm metal nanoparticles. Localized surface plasmons (LSPs) are the result of the confinement of surface plasmons in nanoparticles of size comparable to or smaller than the wavelength of light used to excite the plasmon.[5]

Plasmonics is the emerging field that has yielded methods for guiding and localizing light at the nanoscale by utilizing surface plasmons. Metallic nanostructures and nanoparticles are used to support surface plasmons in three ways: light scattering (**Figure 4a**), light concentration (localized surface plasmons, LSPs) (**Figure 4b**), and light trapping (surface plasmon polaritons, SPPs) (**Figure 4c**).[5] Metallic nanoparticles can be utilized as either subwavelength scattering elements to couple and trap propagating plane waves (**Figure 4a**) or subwavelength antennas to increase light absorption (**Figure 4b**).[6] Unlike metallic nanoparticles, metallic nanostructures like a corrugated metallic film can be used as a supporting layer to couple the incident light into SPP modes (**Figure 4c**).[7]

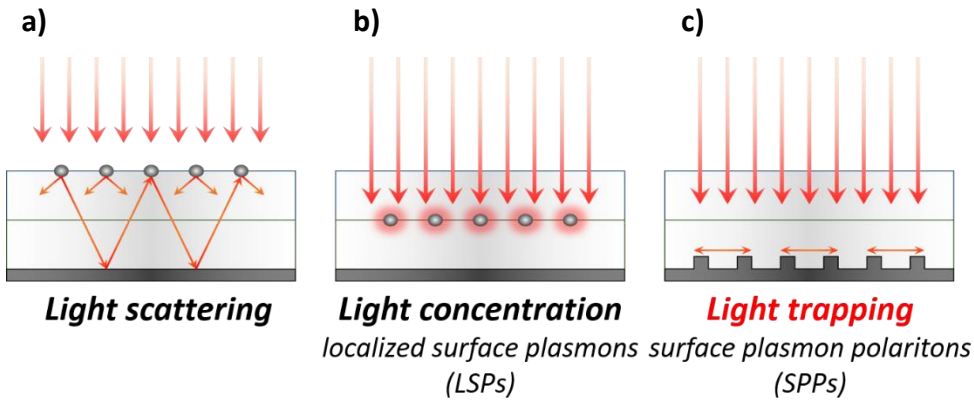

Figure 4. Plasmonic light-trapping geometries. a) light trapping by scattering from metal nanoparticles. **b)** light trapping by the excitation of localized surface plasmons in metal nanoparticles embedded in the interface. **c)** light trapping by the excitation of surface plasmon polaritons at the interface between metallic nanostructures and another layer

1.3 Reflective Display

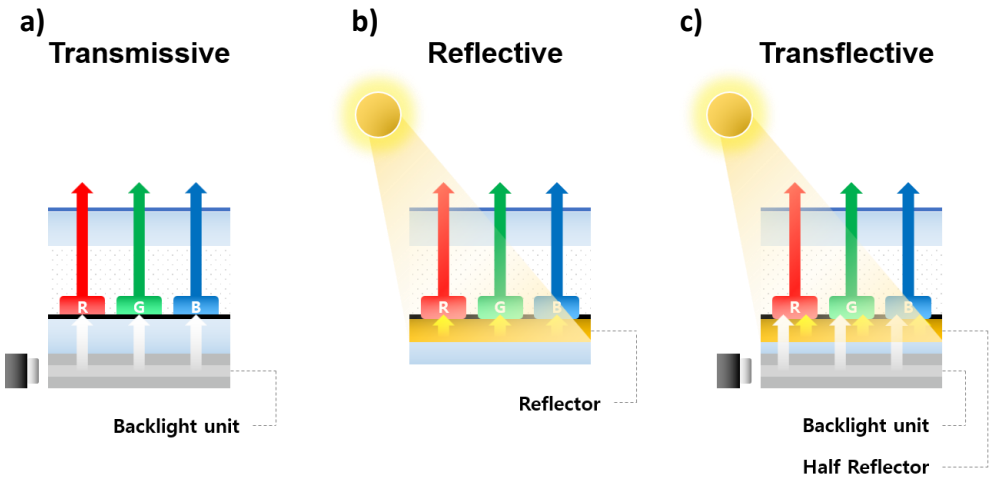

Figure 5. Basic structures and working principles. a) transmissive, **b)** reflective, and **c)** transflective display

Standard transmissive displays depend on a backlight as the light source to illuminate the display (**Figure 5a**). This means that the displays work well indoors where there is lower light but they perform poorly outdoors due to bright sunshine. On the other hand, reflective displays can be operated using an external light source for display luminance, reflecting the light source back to the user via a reflector at the back side of the screen (**Figure 5b**). This means they do not depend on the backlight and reduce the glare from displays and the power needed to run them.[8] Transflective displays combine the features of both transmissive and reflective displays by applying both a half reflector and a backlight to the device structure (**Figure 5c**).

1.4 Basic Concepts: Electromagnetic Waves and Types of Polarization

Electromagnetic waves are periodic changes of electric and magnetic fields in space and time. They propagate at the speed of light. At any point of light, the electric field is always perpendicular to the magnetic field. Both the electric and magnetic fields oscillate in a plane perpendicular to the direction of propagation of the light.

If the electric field (measured at a fixed location of space) oscillates along the straight line, the waves are called *linearly polarized* or *plane-polarized waves* (**Figure 6**).[9]

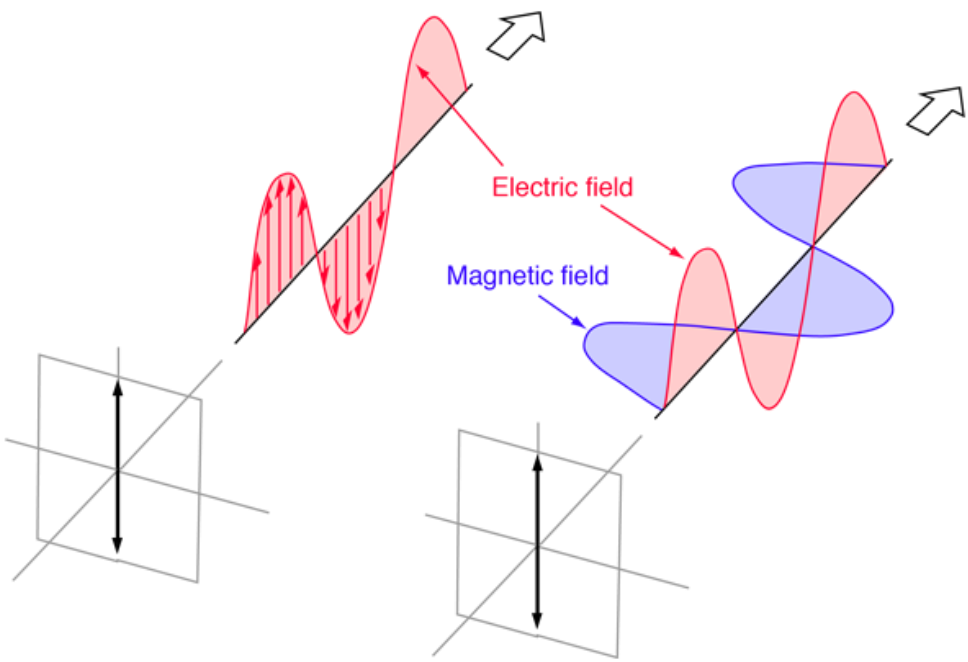

Figure 6. Plane-polarized or linearly polarized wave. The electric field of linearly polarized light is confined to the y-z plane (left) along the direction of propagation

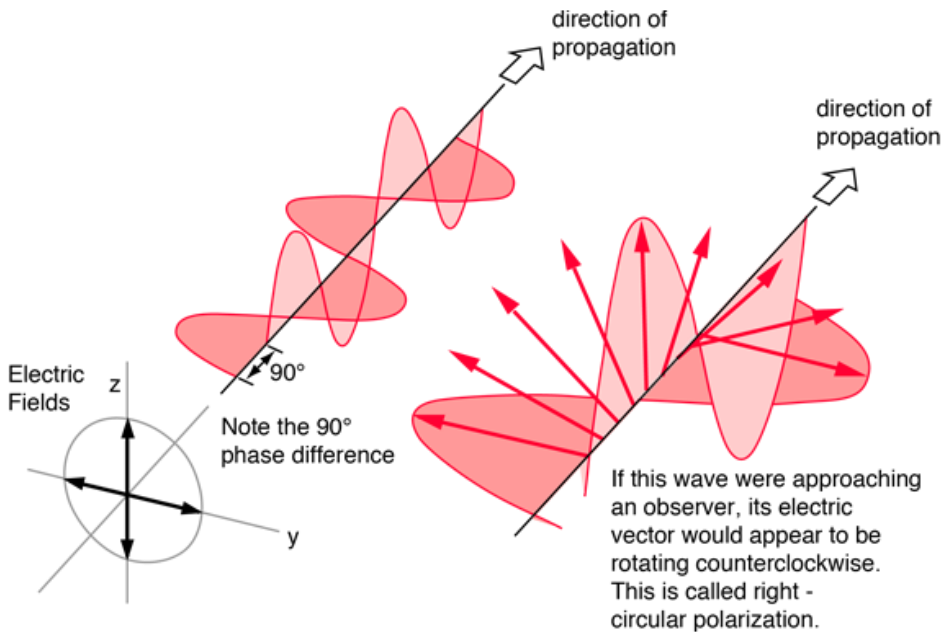

Figure 7. Circularly polarized wave. The circular electric field has two components which are of equal amplitude and have a 90° phase difference. If the two components, however, have differing amplitudes, or if there is a phase difference other than 90°, then they will create elliptically polarized light.

When two linearly polarized waves, perpendicular to each other, are present simultaneously, then the electric fields are added according to the rules of vector addition (superposition). The properties of the resulting wave depend on the intensities and phase difference of the component waves. For example, the superposition of two waves that not only have exactly the same amplitude and wavelength but also are polarized in two perpendicular planes oscillate in the same phase. Its plane of polarization forms a 45° angle with the polarization planes of the component waves. On the other hand, when two

linearly polarized waves, perpendicular to each other, meet out of phase, then the resultant wave will not be linearly polarized wave any more. If there is a phase difference of 90° between two linearly polarized waves, the resultant wave rotates in a circle. Such waves, depending on the rotation direction (clockwise or counterclockwise) are called *left- or right-hand circularly polarized waves* (*L*- or *R*-CPL) (**Figure 7**).[9] The superposition of two circularly polarized light can result in various outcomes. The most interesting result is obtained when a *L*-CPL and a *R*-CPL are added. The resultant wave is a linearly polarized light. That is, any linearly polarized light can be obtained as a superposition of a *L*-CPL and a *R*-CPL, whose amplitude is identical.

1.5 Interaction between light and matter

If light propagates into matter, its properties might alter. Its amplitude, velocity, wavelength, polarization, etc, may change. Two of the basic phenomena of the interaction between light and matter are absorption and a decrease in velocity.

Absorption means that the intensity of light, the square of amplitude, decreases in matter because matter absorbs a part of the light. When the light propagates into the matter, its intensity decreases according to an exponential function inside the matter. After exiting the material, the light oscillates the same way as before entering it but its amplitude is much smaller than it was.

Some materials (chiral compounds) or structures (chiral structures) possess a special property: they absorb *L*-CPL to a different extent in comparison with the absorption of *R*-CPL. This phenomenon is called *circular dichroism* (CD).[10] As discussed above, any linearly polarized light can be obtained as the superposition of a *L*-CPL and a *R*-CPL. Therefore, if linearly polarized light passes through a matter that exhibits circular dichroism, its properties will change because the matter absorbs the two CPL to a different extent.

$$\Delta A = A_L - A_R$$

This differential absorption results in the L-CPL and R-CPL having different amplitudes, which means the superposition wave of the two CPL is no longer linearly polarized. The resultant wave is called *elliptically polarized*.[9]

The decrease in velocity of light in matter is caused by the fact that all materials have a refraction index, which means that the velocity of light is smaller in them than in vacuum. The refraction index is the ratio of the velocities of light measured in vacuum and in the provided material. When the light enters the matter, it slows down because the refracting index of the material is higher than 1.0. Its frequency does not change, therefore, its wavelength decreases. This is because the product of the frequency and the wavelength should be equal to the velocity of light. After that, when the light exits the material, its velocity and wavelength return to the original values (vacuum).

There are materials that possess another special property: their refraction index is different for *L*-CPL and *R*-CPL. This is called *circular birefringence* (CB).[10] As discussed above, any linearly polarized light can be obtained as the superposition of a *L*-CPL and a *R*-CPL. Therefore, if linearly polarized light enters a matter that shows circular birefringence, its properties will alter because of the different extent of the slowdown in *L*-CPL and *R*-CPL. After exiting the matter, the oscillation axis of the resultant light is rotated compared to that of the previous one. In other words, circular birefringence rotates the plane of polarization of linearly polarized light.

1.6 Background of Research

As aforementioned, chiral molecules interact differently with circularly polarized light with opposite handedness (i.e., left- and right-handedness). That is why CD spectroscopy is a very powerful tool for studying chiral molecules. However, the interaction between chiral molecules and circularly polarized light is generally very weak.[2] This problem limits the sensitivity in chirality detection. To overcome this limitation, many researchers have introduced plasmonics to chirality detection. Such efforts opened a new field coined *chiral plasmonics*.

Unlike natural chiral molecules, artificial chiral plasmonic systems strongly interact with circularly polarized light. They can generate very strong chiral plasmonic near-field, leading to enhanced chiral light-matter interactions. With the advancement of nanotechnology over the last few years, it is now possible to create chiral plasmonic nanostructures from planar (or two dimensional, 2D) structures[11,12] to metasurfaces[13,14], a kind of artificial sheet material with sub-wavelength thickness, and three dimensional (3D) structures.[15-18] Compared to 2D chiral plasmonic structures, 3D chiral plasmonic structures typically show stronger chiral light-matter interactions. This is because chiral light-matter interaction in 2D chiral plasmonic structures mainly come from the substrate which could induce a small perturbative symmetry-breaking effect. In addition, when there is no substrate or when the 2D structure is embedded into other uniform matrix, the chirality of the 2D chiral plasmonic structures will disappear.[2]

Various types of top-down and bottom-up strategies have been reported for the fabrication of chiral plasmonic nanostructures. Most of top-down approaches have been accomplished by using electron beam lithography,[19] nanohole lithography,[20] holographic lithography,[21] grazing incident deposition,[22] and nano-template assisted deposition.[23] Such techniques have big advantages in accuracy in relation to the sizes and shapes of the complicated structures. However, the fabrication processes take longer than other methods because of the several required steps and are not efficient in cost for large-scale structures. Bottom-up fabrication methods, especially self-assembly, have also been reported using chiral molecular templates including DNA or peptide.[24] These methods are more efficient in the fabrication of 3D chiral plasmonic nanostructures. However, most of these methods inevitably need highly purified chiral molecules, which usually cost so much. Hence, the fabrication of artificial chiral structures from intrinsically achiral materials is still very challenging.

In this work, we report a facile fabrication method for 3D chiral plasmonic structure induced by asymmetric biaxial stretching with nanoscale grating-patterned PDMS films. Asymmetric biaxial stretching processes are a little different from the method reported previously by Han and co-worker.[25] The 3D chiral plasmonic structures have nanoscale grating patterns, nanoscale wrinkled patterns, and microscale chiral wrinkled patterns, simultaneously. Finally, potential applications of the 3D chiral plasmonic patterned PDMS film to reflective display were explored.

Chapter 2. Experimental

2.1 Fabrication of Grating-Patterned PDMS Film

A grating-patterned PDMS film was obtained by pouring a PDMS precursor solution (1:10 ratio of curing agent to silicone elastomer) onto a grating mold (Thorlabs, GR25-1850) and curing at 70℃ for 2 h. The PDMS film was then lifted off from the mold (**Figure 8**). The grating-patterned PDMS film had a thickness of approximately 350 ㎛.

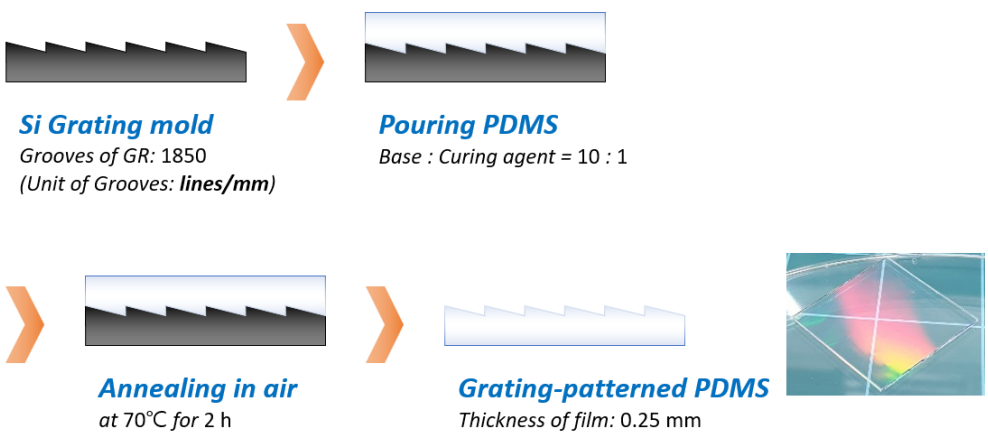

Figure 8. Schematic procedure of the fabrication of grating-patterned PDMS film.

2.2 Fabrication of 3D Chiral Plasmonic-Patterned Film

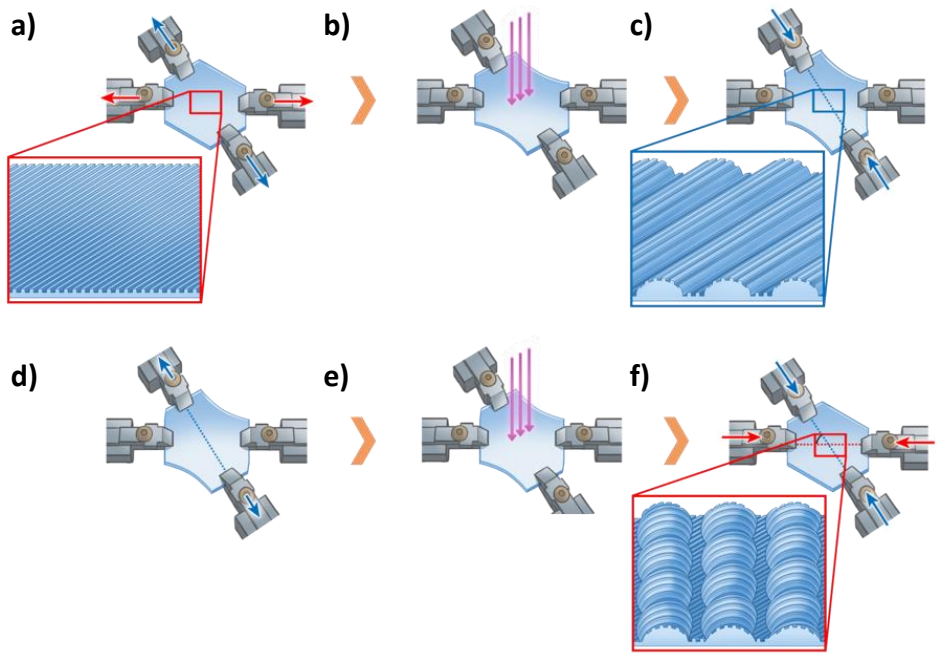

Figure 9. Schematic procedure of the fabrication for 3D chiral plasmonic patterns. a) a grating-patterned PDMS film is stretched with asymmetrical and biaxial strains of ε = 30%. **b)** O_2 plasma treatment & first UV/Ozone exposure for 60 min to form a SiO_x layer on the surface of the film. **c)** release of the main axis (blue arrows) induces wrinkled structures perpendicular to the main axis. **d)** re-stretch along the main axis to flatten the film. **e)** second UV/Ozone exposure for 45 min to form thicker SiO_x layers. **f)** release of both the main axis (blue arrows) and sub axis (red arrows), sequentially to prepare the 3D chiral plasmonic-patterned wrinkles.

A custom-made biaxial strain controllable stage was used to stretch the grating-patterned PDMS film. After putting the PDMS film on the stage, the film was first stretched in the direction of the sub axis and then subsequently stretched in the direction of the main axis. The angle between the two axes (θ)

was 60° for one samples and 120° for the other samples. The strain ($\varepsilon = (L-L_0)/L_0$, where L_0 is the initial length before stretching, and L is the length after stretching) along each axis were adjusted to 30%. Then, O_2 plasma treatment was conducted to modify the surface (Femto science, VITA). Then, the samples were exposed to UV/Ozone (AhTech LTS Corp., AC-3) for 60 min to form a SiO_x layer on the surface of the film. Next, the uniaxial strain along the main axis was fully released to form the first wrinkles. The first released films were re-stretched along the main axis to flatten the films. Plus, the films were exposed once more to UV/Ozone for 45 min to form thicker SiO_x layers on top of the films. Finally, all strains were released to prepare the 3D chiral plasmonic-patterned wrinkles (**Figure 9**). After the formation of the 3D chiral plasmonic patterns, 3 nm-thick Cr and 30 nm-thick Au layers were thermally deposited onto the film under a vacuum ($<10^6$ Torr).

2.3 Fabrication of 3D Reflective Display

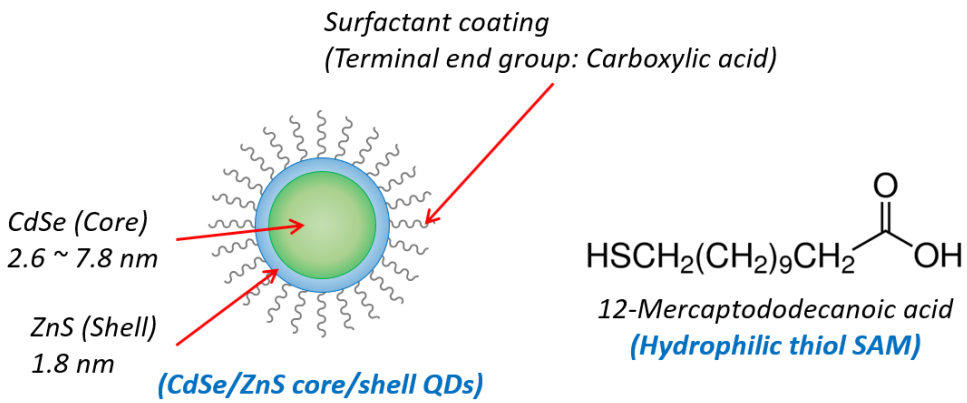

Figure 10. Schematic image of quantum dots (left) and self-assembled monolayer (right).

Two kinds of CdSe/ZnS core/shell quantum dots (QDs) solution (25% (v/v) in DI water) were purchased from Nano Optical Materials Inc. They emit red (emission peak center: 660 nm) and green (emission peak center: 540 nm). QDs have surfactant terminal end groups that are a carboxylic acid. Since other organic solvents can swell PDMS film, we chose QDs that are distributed in DI water.[26] 12-mercaptoundecanoic acid (MUDA), which is hydrophilic thiol SAM, was purchased from Sigma Aldrich (**Figure 10**).

The SAMs of MUDA were achieved by pouring 10 mM MUDA ethanol solution on the gold surface of the sample for 30 min at room temperature. After that, it was rinsed with DI water. QD solution was dropped onto the surface of the sample. QDs on the MUDA SAM treated gold surface was bound by hydrogen bonds (**Figure 11**).[27]

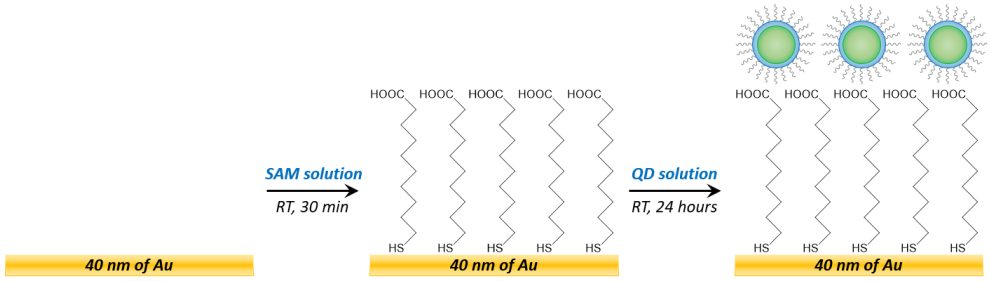

Figure 11. Schematic procedure for coating QDs onto Au film.

2.3 Morphological Characterization of 3D Chiral Plasmonic Patterns

SEM images were obtained using a FE-SEM (ZEISS, MERLIN Compact). OM images (Olympus, BX53M) were captured to analyze the surface of the patterned PDMS films. 3D surface profiler (NanoFocus, μSurf) was used to measure the 3D topologies of the chiral plasmonic-patterned films.

2.4 Optical Characterization of 3D chiral plasmonic patterned films

The optical absorption and CD spectrum were obtained using a circular dichroism spectropolarimeter (JASCO, J-815 150L). The photoluminescence (PL) characteristics were studied using a Xe lamp coupled to a 300 nm monochromator. A 420 nm picosecond laser diode with an 80 MHz repetition rate was used as an excitation source. Time-resolved photoluminescence (TRPL) spectra were measured using a time-correlated single photon counting (TCSPC) method. A commercially available TCSPC module (PicoQuant, Germany) was used to obtain the PL decay curves.

UV-vis spectra of the films were recorded with 150 mm integrating spheres by generating circularly polarized light (JASCO, V-770). Circularly polarized light was generated by placing an extra linear polarizer and quarter-wave plate (Thorlabs) on the pathway from the light source to the samples.

The quantum efficiency of fluorescence was measured on a quantum yield measurement system (Otsuka Photal Electronics, QE-2100).

Chapter 3. Results and Discussions

3D CPPs were fabricated via two steps: 1) fabrication of nano-scale grating-patterned PDMS film, 2) the sequential formation of micro-scale wrinkled patterns with designated directions in the grating-patterned PDMS film. The handedness of the 3D CPPs can be easily controlled by adjusting the angle (θ) between the main and sub axis. The 3D CPPs fabricated with θ = 60° are denoted as right-handed (RH) and those with θ = 120° are denoted as left-handed (LH).

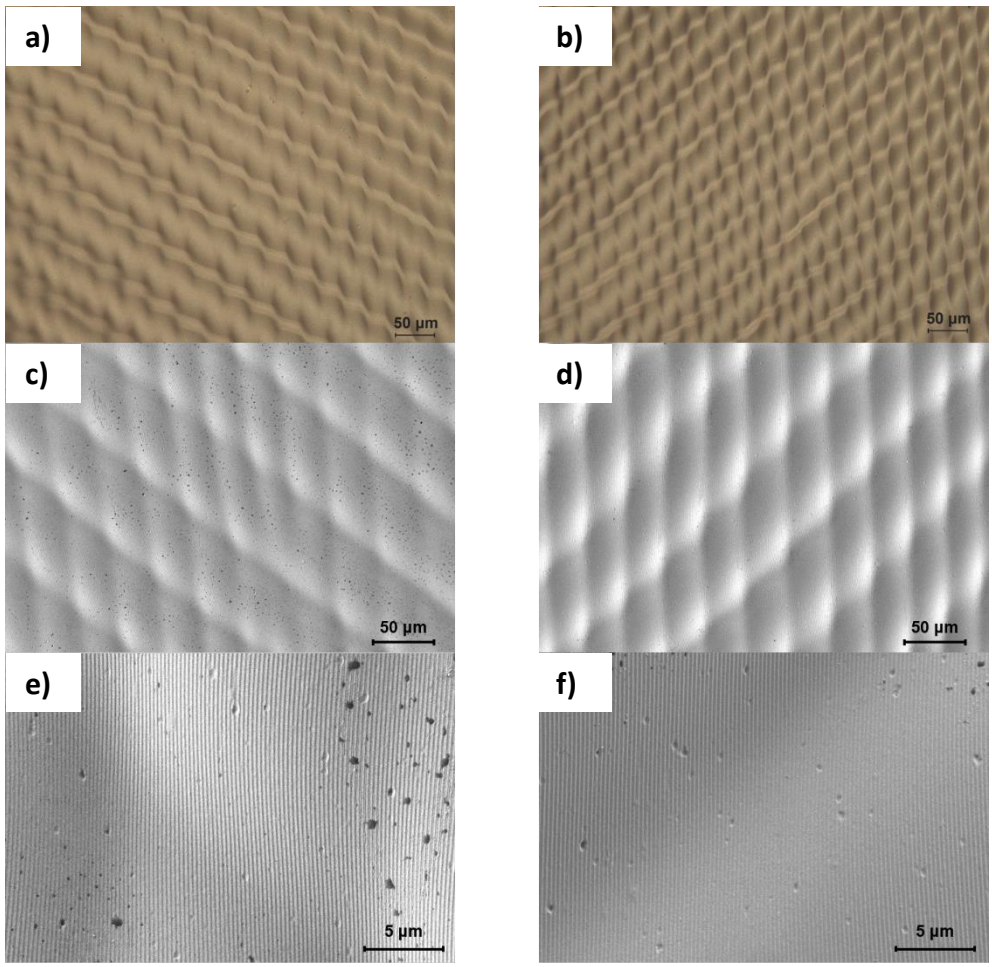

Figure 12. optical microscopy images & SEM images of 3D CPPs (RH sample: left, LH sample: right). a, b) optical microscopy images and **c, d)** SEM images of micro-scale patterns, **e, f)** SEM images of nano-scale patterns

Micro-scale 3D chiral patterns of the samples can be clearly seen in **Figure 12a ~ 12d**. Then, since it should be confirmed that nano-scale grating patterns are not broken, we obtained higher resolution scanning electron microscope (SEM) images of 3D CPPs, as shown in **Figure 12e & 12f**.

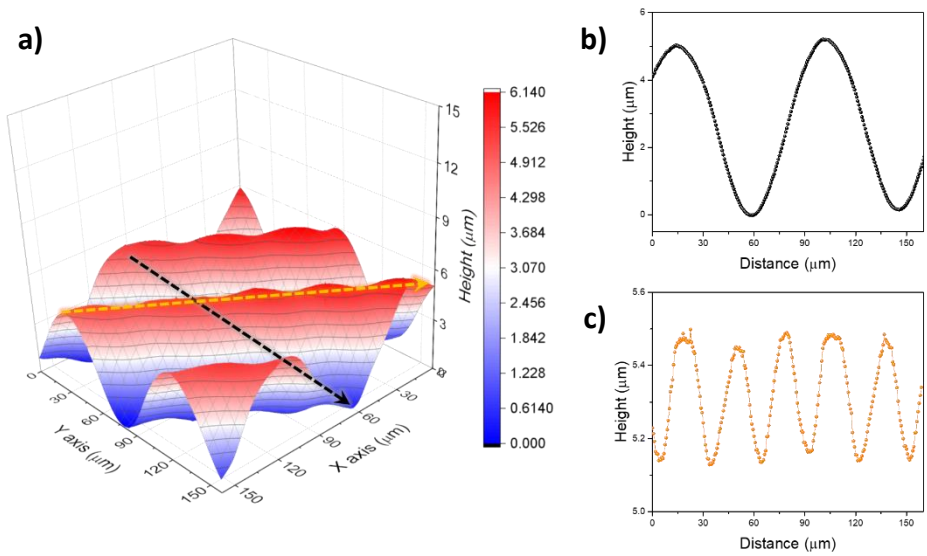

Figure 13. 3D optical profiler image & Depth profiles of 3D chiral plasmonic structures. a) 3D optical profiler image, the right side of the figure includes a colorimeter band representing the height of each spot as different color, **b, c)** depth profiles of 3D plasmonic structures along black and orange lines

The 3D CPPs were scanned using a 3D optical profiler (**Figure 13a**) to calculate their periodicity and amplitude. The depth profiles of RH sample were scanned along the maxima of the oscillations (**Figure 13a**), and are shown as black and orange lines in **Figure 13b**, **c**, respectively. The depth profiles exhibit periodic oscillations with periodicity values of 87.2 ± 1.2 μm (black) and 29.5 ± 1.6 μm (orange) and show amplitudes of 5.06 ± 0.01 μm (black) and 0.42 ± 0.09 μm (orange). The depth profiles of LH sample do not show exactly the same values as those of RH sample.

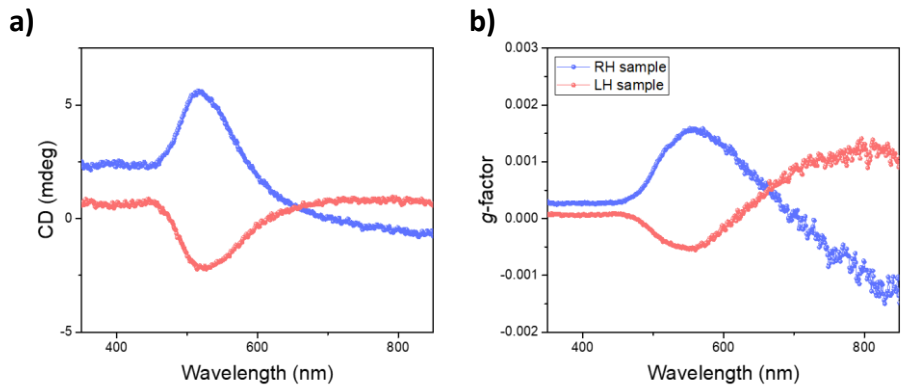

Figure 14. CD spectra and *g*-factor of only micro-scale chiral patterns. a) circular dichroism spectra and **b)** dissymmetry *g*-factors (right) of both the RH (blue) and LH (red) sample with only micro-scale chiral patterns

At first, we investigated how each pattern affects the CD spectra. Circular dichroism spectroscopy confirms the formation of micro-scale patterns (**Figure 14a**). The measured circular dichroism spectra were inverted with respect to each other, but had almost the same peak positions at 516 nm (RH sample, blue) and 527 nm (LH sample, red). Their maximum CD values were 5.63 and -2.23 mdeg in RH and LH sample, respectively. The *g*-factor of only micro-scale chiral patterns was lower than 0.002, as shown in **Figure 14b**. Secondly, CD spectra of 3D CPPs were measured (**Figure 15a**). Nano-scale grating patterns could cause light trapping at the metal/air interface by the excitation of SPPs. That is expected to enhance both CD value and *g*-factor of 3D CPPs.

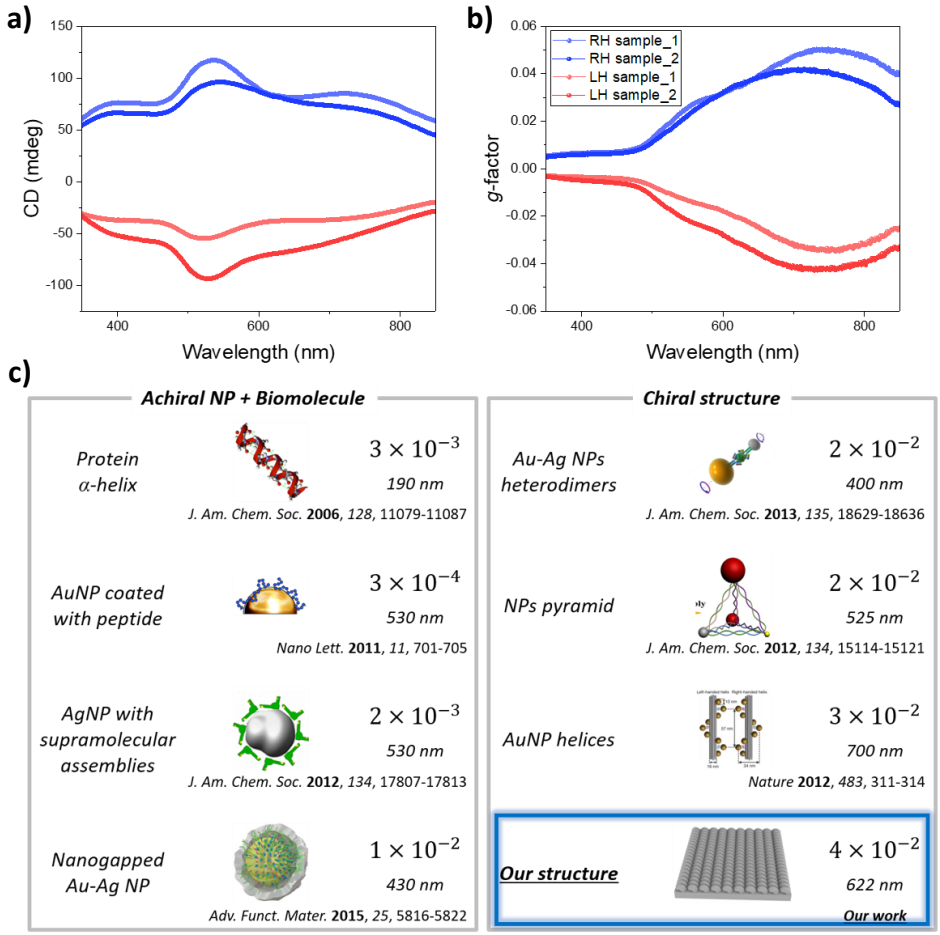

Figure 15. CD spectra and *g*-factor of 3D CPPs. a) circular dichroism spectra and **b)** dis-symmetry *g*-factors of both the RH (blue) and LH (red) 3D CPPs, **c)** comparison of the dis-symmetry *g*-factors of the 3D CPPs and other works

CD spectroscopy confirms the enhancement effect of 3D CPPs (**Figure 15a**). The measured CD spectra were inverted with respect to each other, but had almost the same peak positions, at 537 nm (RH sample, blue) and 528 nm (LH sample, red). This is because RH sample and LH sample were not exactly the same periodicity and amplitudes of their patterns. As we expected, the

maximum value of CD was increased up to 117.4 (RH sample, blue) and -93.8 mdeg (LH sample, red) by two orders of magnitude due to the light trapping by the excitation of SPPs. The *g*-factors of 3D CPPs exhibit the values over ~0.04 at 657 nm (RH sample, blue) and 682 nm (LH sample, red), which is one of the highest values in chiral structures (**Figure 15b**).[17,28,29] The *g*-factors of various chiral nanostructures are compared in **Figure 15c**.[17,28-32] As it can be seen, our 3D CPPs show the highest *g*-factor. It could be attributed to densely formed chiral patterns. Unlike other chiral structures, our structures are densely and regularly formed over the large area.

As investigated before, the CD spectra of 3D chiral structures with only micro-scale chiral patterns were measured to confirm the difference in intensity of CD spectra depending on with and without nano-scale grating pattern. However, the intensity of their CD spectra were stronger than it would be expected. To investigate the 3D CPPs in more detail, the unit cell of the 3D CPPs (RH sample) is defined as shown in **Figure 16b**. It was divided into 9 regions (**Figure 16c**) and SEM images of each part were obtained (**Figure 16d**). As shown in **Figure 16d**, there were unexpected patterns which repeat approximately 110 nm. We attribute the strong intensity of CD spectra of 3D chiral structures with only micro-scale chiral patterns to the 110 nm patterns. Long, thick, and irregular lines, running from the upper left side to the lower right side, are cracks. The formation of a hard SiO_x layer on the PDMS surface by surface treatment such as UV/Ozone and O_2 plasma treatment can often lead to surface deformations such as both these cracks and wrinkles owing to

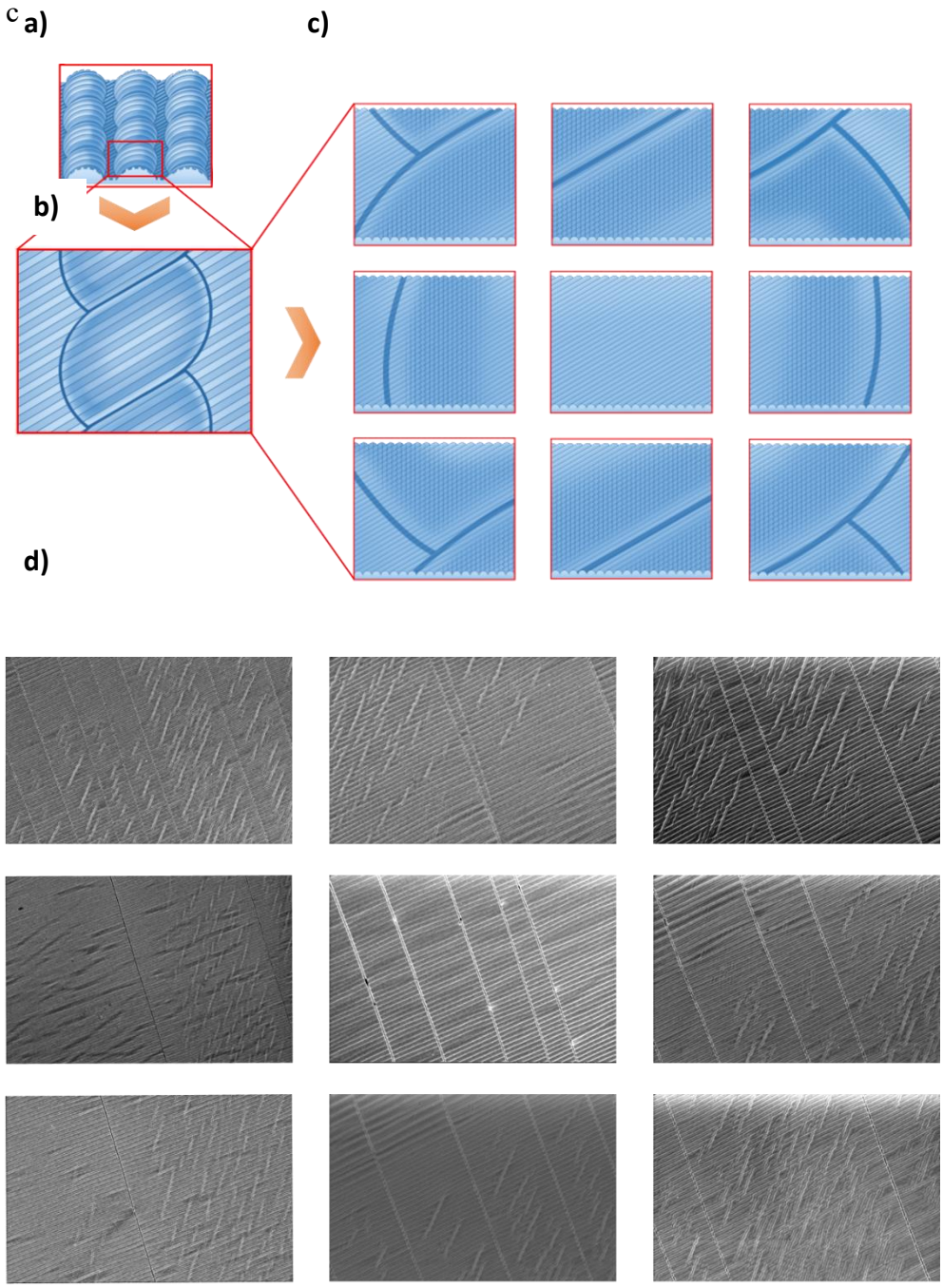

Figure 16. Schematic images and SEM images of each part of unit cell. a-c) definition of unit cell of 3D chiral plasmonic patterns and its each part, **d)** SEM images of each part of unit cell

the strain mismatch generated by thermal stress from a difference in the coefficient of thermal expansion (CTE) or interfacial stress from the alteration of chemical structures.[33] However, our PDMS film was biaxially pre-stretched. As releasing each axis after the first and second UV/Ozone exposure, the wrinkles due to the strain mismatch were aligned parallel to the releasing each axis, respectively. As a result of these processes, the 110 nm patterns parallel to each axis could be formed.

Through CD spectroscopy and surface investigation (OM, 3D surface profiler, and SEM), we were able to confirm that our 3D CPPs differently interact with *R*-CPL and *L*-CPL. However, it is hard to know intuitively. Some researchers have reported their works that show changes in optical properties due to the interaction between light and matter as changes in current of optoelectronic devices[34,35] or intensity of luminescence.[36] Different from these approaches, we tried to develop a new strategy, in which our patterns are used for reflective displays, in order to detect CPL through changes in color.

First of all, UV/vis spectroscopy using circularly polarized light as light source was necessary. Therefore, polarizer and retarder (or quarter wave plate) were located in the light pathway between light source and sample (**Figure 17**). UV/vis spectra were consistent with what we expected. RH sample showed relatively higher reflectance of *R*-CPL than that of *L*-CPL (0.591% at 660 nm, 0.52% at 540 nm, 0.969% at 460 nm in RH sample), while LH sample showed the opposite result (0.343% at 660 nm, 0.449% at 540 nm

0.745% at 460 nm in LH sample) (**Figure 18**). Based on these results, we tried to fabricate a reflective display that changes the color according to the CPL.

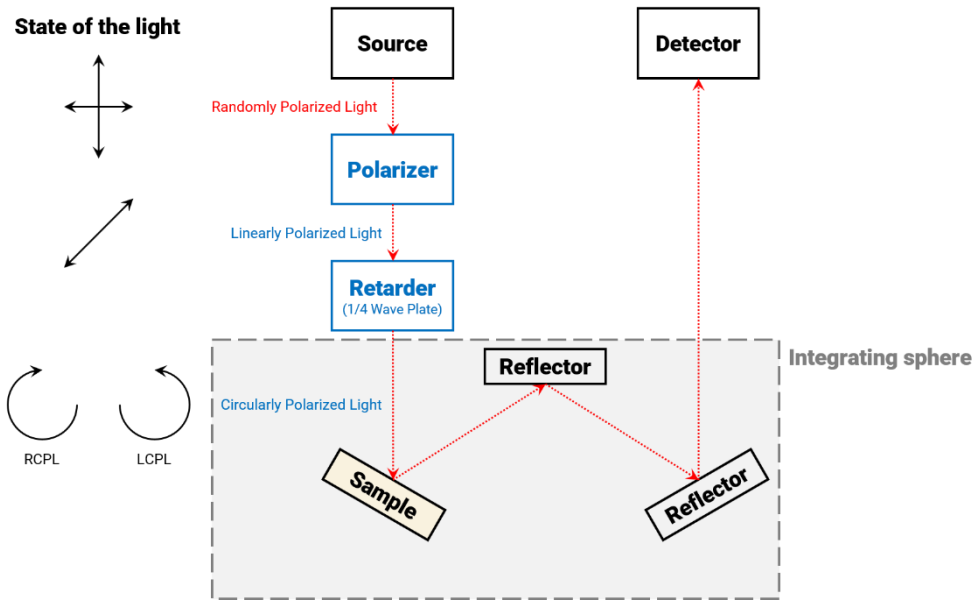

Figure 17. Schematic of UV/vis spectroscopy experimental set-up. To transform unpolarized light into circularly polarized light, extra polarizer and retarder are put on the light pathway between light source and sample

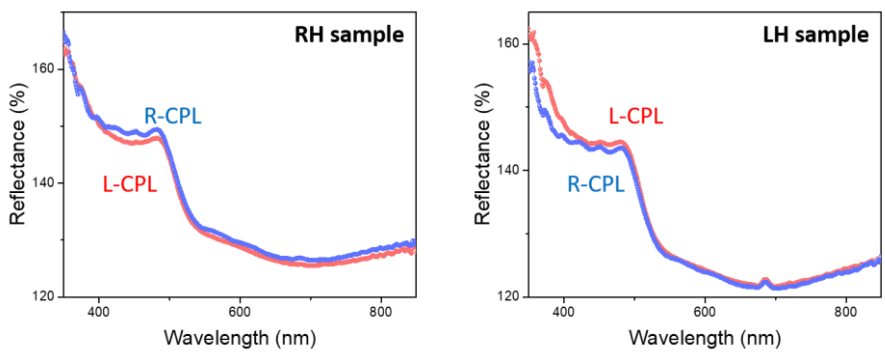

Figure 18. UV/vis spectra. RH (left) and LH (right) sample, respectively

In the beginning, we decided to examine the change in the photoluminescence intensity of quantum dots (QDs). Therefore, we applied one kind of QDs (green, emission wavelength: 660 nm) onto RH and LH sample as a light emitter and fabricated a reflective display based on the 3D CPPs. The QDs had to be water soluble because there is high chance of PDMS film absorbing other solvents and swelling.[26] Detailed experimental methods are explained in **Chapter 2.3**. Photoluminescence (PL) spectra were measured using the set-up shown in **Figure 19**. PL spectra exhibited the same result as what we expected. RH sample showed a higher intensity of *R*-CPL than that of *L*-CPL, whereas LH sample showed the opposite result (**Figure 20**). However, there were very little differences. From the point of view of reflectance, they should have shown much greater difference. That might be due to thick QD layer on the functionalized Au surface. As the QD layer became thicker, the more scattering could occur, and this result indicates that the less incident light would reach the surface of 3D CPPs coated with Au.

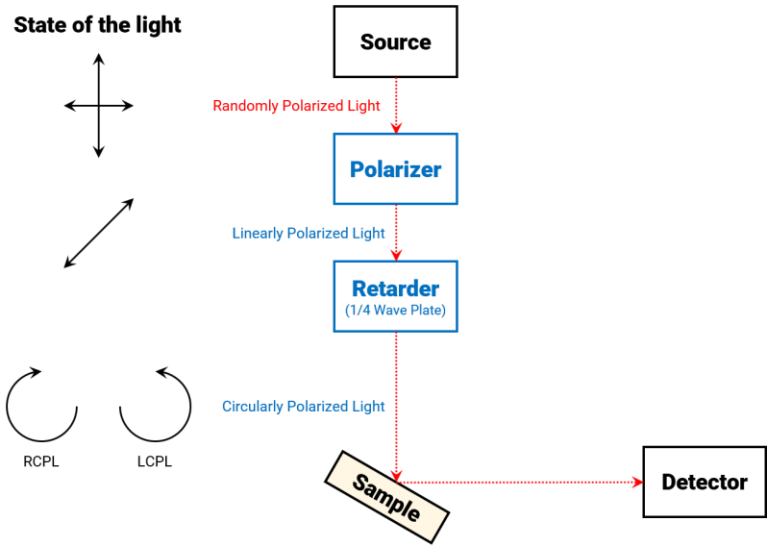

Figure 19. Schematic of photoluminescence (PL) experimental set-up. To transform randomly polarized light into circularly polarized light, extra polarizer and retarder are put on the light pathway between light source and sample

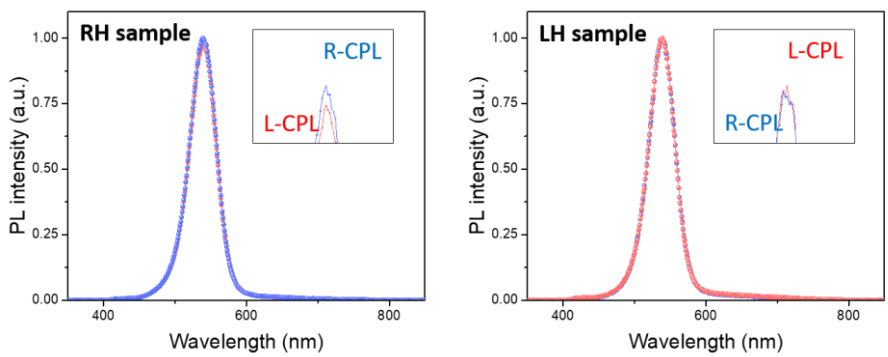

Figure 20. Photoluminescence (PL) spectra. RH (left) and LH (right) sample, respectively

Chapter 4. Conclusion

In conclusion, we fabricated 3D chiral plasmonic structures (CPPs) by symmetric biaxial stretching with nano-scale grating-patterned PDMS film. The novel 3D CPPs had micro-scale chiral patterns, nano-scale grating patterns, and other nano-scale irregular patterns. The effect of each pattern on the CD spectra were investigated. Only micro-scale chiral patterns were able to cause chiroptical responses with the corresponding intensity of 5.63 mdeg. The 3D CPPs, which had not only micro-scale chiral patterns but also nano-scale grating patterns, exhibited the enhanced CD value up to 117.4 mdeg and *g*-factor over 0.04, which is among the highest values, to the best of our knowledge. Also, the 3D CPPs exhibited differences in reflectance (0.591% at 660 nm, 0.343% at 660 nm in RH and LH sample, respectively) according to *R*-CPL and *L*-CPL. Based on these results, the 3D CPPs were analyzed for potential applications for reflective display. However, there were very little differences of PL intensities between RH and LH sample. That might be due to thick QD layer on the functionalized Au surface. The thicker QD layer causes the more scattering, indicating that the less incident light could reach 3D CPPs coated with Au. Incorporating 3D CPPs as a back reflector in reflective display has shown the possibility that changes in optical properties can be seen as a color change, due to the different interactions between the structures and either left-handed or right-handed circularly polarized light.

References

1 Hentschel, M., Schäferling, M., Duan, X., Giessen, H. & Liu, N. Chiral plasmonics. *Science Advances* **3**, e1602735, doi:10.1126/sciadv.1602735 (2017).

2 Du, W., Wen, X., Gérard, D., Qiu, C.-W. & Xiong, Q. Chiral plasmonics and enhanced chiral light-matter interactions. *Science China Physics, Mechanics & Astronomy* **63**, 244201, doi:10.1007/s11433-019-1436-4 (2019).

3 Wade, L. G. & Simek, J. W. *Organic Chemistry*. (Pearson, 2017).

4 Gal, J. Louis Pasteur, language, and molecular chirality. I. Background and Dissymmetry. *Chirality* **23**, 1-16, doi:https://doi.org/10.1002/chir.20866 (2011).

5 Maier, S. A. *Plasmonics: Fundamentals and Applications*. (Springer US, 2007).

6 Bohren, C. F. How can a particle absorb more than the light incident on it? *American Journal of Physics* **51**, 323-327, doi:10.1119/1.13262 (1983).

7 Atwater, H. A. & Polman, A. Plasmonics for improved photovoltaic devices. *Nature Materials* **9**, 205-213, doi:10.1038/nmat2629 (2010).

8 Heikenfeld, J., Drzaic, P., Yeo, J.-S. & Koch, T. Review Paper: A critical review of the present and future prospects for electronic paper. *Journal of the Society for Information Display* **19**, 129-156, doi:https://doi.org/10.1889/JSID19.2.129 (2011).

9 Hecht, E. *Optics*. (Pearson Education, Incorporated, 2017).

10 Woody, R. W. in *Methods in Enzymology* Vol. 246 34-71 (Academic Press, 1995).

11 Zu, S., Bao, Y. & Fang, Z. Planar plasmonic chiral nanostructures. *Nanoscale* **8**, 3900-3905, doi:10.1039/C5NR09302C (2016).

12 Zhang, C., Li, Z.-Q., Yang, X., Chen, Z. & Wang, Z. Controlling third harmonic generation with gammadion-shaped chiral metamaterials. *AIP Advances* **6**, 125014, doi:10.1063/1.4971375 (2016).

13 Wang, Q. *et al.* Reflective chiral meta-holography: multiplexing holograms for circularly polarized waves. *Light: Science & Applications* **7**, 25, doi:10.1038/s41377-018-0019-8 (2018).

14 Li, W. *et al.* Circularly polarized light detection with hot electrons in chiral plasmonic metamaterials. *Nature Communications* **6**, 8379, doi:10.1038/ncomms9379 (2015).

15 Ogier, R., Fang, Y., Svedendahl, M., Johansson, P. & Käll, M. Macroscopic Layers of Chiral Plasmonic Nanoparticle Oligomers from Colloidal Lithography. *ACS Photonics* **1**, 1074-1081, doi:10.1021/ph500293u (2014).

16 Gansel, J. K. *et al.* Gold Helix Photonic Metamaterial as Broadband Circular Polarizer. *Science* **325**, 1513-1515, doi:10.1126/science.1177031 (2009).

17 Kuzyk, A. *et al.* DNA-based self-assembly of chiral plasmonic nanostructures with tailored optical response. *Nature* **483**, 311-314, doi:10.1038/nature10889 (2012).

18 Dietrich, K. *et al.* Elevating optical activity: Efficient on-edge lithography of three-dimensional starfish metamaterial. *Applied Physics Letters* **104**, 193107, doi:10.1063/1.4876964 (2014).

19 Hentschel, M., Ferry, V. E. & Alivisatos, A. P. Optical Rotation Reversal in the Optical Response of Chiral Plasmonic Nanosystems: The Role of Plasmon Hybridization. *ACS Photonics* **2**, 1253-1259, doi:10.1021/acsphotonics.5b00354 (2015).

20 Frank, B. *et al.* Large-Area 3D Chiral Plasmonic Structures. *ACS Nano* **7**, 6321-6329, doi:10.1021/nn402370x (2013).

21 Pang, Y. K. *et al.* Chiral microstructures (spirals) fabrication by holographic lithography. *Opt. Express* **13**, 7615-7620, doi:10.1364/OPEX.13.007615 (2005).

22 Yang, L. *et al.* Chiral Nanoparticle-Induced Enantioselective Amplification of Molecular Optical Activity. *Advanced Functional Materials* **29**, 1807307, doi:https://doi.org/10.1002/adfm.201807307 (2019).

23 Yeom, B. *et al.* Chiral Plasmonic Nanostructures on Achiral Nanopillars. *Nano Letters* **13**, 5277-5283, doi:10.1021/nl402782d (2013).
24 Lee, H.-E. *et al.* Amino-acid- and peptide-directed synthesis of chiral plasmonic gold nanoparticles. *Nature* **556**, 360-365, doi:10.1038/s41586-018-0034-1 (2018).
25 Hwang, M., Kim, C., Kim, J., Son, J. G. & Yeom, B. Controlled Fabrication of 3D Chiral Microwrinkles via Asymmetrical and Biaxial Bucklings. *Advanced Functional Materials* **29**, 1808979, doi:https://doi.org/10.1002/adfm.201808979 (2019).
26 Koschwanez, J. H., Carlson, R. H. & Meldrum, D. R. Thin PDMS Films Using Long Spin Times or Tert-Butyl Alcohol as a Solvent. *PLOS ONE* **4**, e4572, doi:10.1371/journal.pone.0004572 (2009).
27 Song, Y. *et al.* Immobilization of DNA on 11-mercaptoundecanoic acid-modified gold (111) surface for atomic force microscopy imaging. *Microscopy Research and Technique* **68**, 59-64, doi:https://doi.org/10.1002/jemt.20235 (2005).
28 Wu, X. *et al.* Unexpected Chirality of Nanoparticle Dimers and Ultrasensitive Chiroplasmonic Bioanalysis. *Journal of the American Chemical Society* **135**, 18629-18636, doi:10.1021/ja4095445 (2013).
29 Yan, W. *et al.* Self-Assembly of Chiral Nanoparticle Pyramids with Strong R/S Optical Activity. *Journal of the American Chemical Society* **134**, 15114-15121, doi:10.1021/ja3066336 (2012).
30 Gautier, C. & Bürgi, T. Chiral N-Isobutyryl-cysteine Protected Gold Nanoparticles: Preparation, Size Selection, and Optical Activity in the UV−vis and Infrared. *Journal of the American Chemical Society* **128**, 11079-11087, doi:10.1021/ja058717f (2006).
31 Slocik, J. M., Govorov, A. O. & Naik, R. R. Plasmonic Circular Dichroism of Peptide-Functionalized Gold Nanoparticles. *Nano Letters* **11**, 701-705, doi:10.1021/nl1038242 (2011).
32 Maoz, B. M. *et al.* Plasmonic Chiroptical Response of Silver Nanoparticles Interacting with Chiral Supramolecular Assemblies. *Journal of the American Chemical Society* **134**, 17807-17813, doi:10.1021/ja309016k (2012).
33 Park, J.-Y. *et al.* Controlled wavelength reduction in surface wrinkling of poly(dimethylsiloxane). *Soft Matter* **6**, 677-684, doi:10.1039/B916603C (2010).
34 Yang, Y., da Costa, R. C., Fuchter, M. J. & Campbell, A. J. Circularly polarized light detection by a chiral organic semiconductor transistor. *Nature Photonics* **7**, 634-638, doi:10.1038/nphoton.2013.176 (2013).
35 Gilot, J. *et al.* Polymer Photovoltaic Cells Sensitive to the Circular Polarization of Light. *Advanced Materials* **22**, E131-E134, doi:https://doi.org/10.1002/adma.200903995 (2010).
36 Yan, J., Wu, S.-T., Cheng, K.-L. & Shiu, J.-W. A full-color reflective display using polymer-stabilized blue phase liquid crystal. *Applied Physics Letters* **102**, 081102, doi:10.1063/1.4793750 (2013).

Abstract in Korean

2차원부터 메타표면, 3차원의 인공 카이랄 구조물은 특별한 광학적 특성을 보여 큰 관심을 받아왔습니다. 하지만, 복잡한 제작 과정과 적용가능한 재료의 한계로 인하여 나노 사이즈를 비롯하여 마이크로 사이즈의 카이랄 구조물조차 실현하는 것이 쉽지 않기에 여전히 문제가 되고 있습니다.

본 연구에서는 나노 사이즈의 격자구조가 새겨진 PDMS 필름을 두 방향으로 늘림으로써 3차원 카이랄 플라즈모닉 구조를 제작하였습니다. 새로운 3차원 카이랄 플라즈모닉 구조는 마이크로 사이즈의 카이랄구조, 나노 사이즈의 격자구조, 그리고 앞선 격자구조와는 다른 나노 사이즈의 불규칙 구조를 갖습니다. 그리고 이 구조를 3차원 반사형 디스플레이에 적용이 가능한지에 대해서 분석하였습니다. 3차원 반사형 디스플레이의 후면 반사기로 이 멀티패턴 구조를 적용하는 것은 구조와 왼쪽 또는 오른쪽 원편광과의 다른 상호작용으로 인한 광학적 특성의 변화를 색상 변화로 나타낼 수 있다는 가능성을 보여주었습니다. 이 방법은 다중패턴 3차원 카이랄 구조의 제작에 널리 사용될 수 있습니다.

주요어: 카이랄성 탐지, 플라즈모닉 효과, 카이랄 플라즈모닉 패턴 반사형 디스플레이

학 번: 2019-29299

Acknowledgement

이 논문을 완성하기까지 정말 많은 분들의 도움을 받았습니다. 가장 먼저, 학위 과정의 시작과 끝을 함께 해주시고, 열정으로 지도해주신 오준학 교수님께 감사의 말씀을 드립니다. 지난 2년의 시간을 돌아보니 교수님의 지도 아래 여기까지 올 수 있었다고 생각합니다. 또한, 바쁘신 와중에도 석사 학위 심사위원으로 자리해주셔서 제 연구를 평가해주시고 좋은 말씀과 더불어 앞으로 나아가야 할 방향에 대해서 소중한 조언을 남겨주신 이종찬 교수님, 유동원 교수님께도 진심으로 감사의 말씀을 드립니다.

공동연구자로 이 연구를 함께 진행한 같은 연구실 출신의 이윤호 박사에게도 감사드립니다. 오준학 교수님께서 포항공과대학교(POSTECH)에 재직하셨던 시절부터 이어져온 소중한 인연 덕분에 그동안 즐겁게 연구할 수 있었습니다. 정말 감사합니다.

제 석사 학위과정 동안 함께 동고동락했던 OPEL 멤버 여러분, 정말 감사드립니다. 뛰어난 역량을 지닌 여러분과 함께 연구를 할 수 있어서 행복했습니다. 그리고 여러분이 평소 뿜어내는 밝은 에너지 덕분에 힘든 학위 과정을 무사히 마칠 수 있었습니다. 정말 감사합니다.

마지막으로, 늘 곁에서 저를 믿고 응원해주시는 가족들에게 이 자리를 빌어 감사의 말씀을 올립니다. 일이 바쁘다는 핑계로 집에 자주 가지도 못하고 전화도 자주 못했던 못난 아들이지만, 그래도 마음만큼은 누구보다 가족을 사랑하고 있다는 걸 알아주셨으면 좋겠습니다. 사랑합니다.